

Highly Sensitive Magnetic Focus FEA Image Sensor with HARP Target

Y. Hirano¹, M. Nanba¹, Y. Honda¹, K. Miyakawa¹, T. Watabe¹, S. Okazaki¹, N. Egami¹,
Y. Obara², M. Tanaka², S. Itoh² and A. Kobayashi³

¹NHK Science & Technical Research Labs, 1-10-11, Kinuta, Setagaya, Tokyo 157-8510, JAPAN

TEL: +81-3-5494-3264, FAX: +81-3-5494-3278, e-mail: hirano.y-eg@nhk.or.jp

²Futaba Co., Chiba 299-4395, JAPAN

³Hamamatsu photonics K.K., Hamamatsu-shi 438-0193, JAPAN

Abstract

A 50×50 μm pixel magnetic focus field emitter array image sensor with a highly sensitive avalanche-mode photoconductive target was fabricated and tested as a step toward the development of ultrahigh-sensitivity compact image sensors for high-definition TV cameras. Our experimental results revealed that the prototype could obtain both high-sensitivity and enough resolution for its pixel size by focusing electrons emitted from the field emitter array onto the highly sensitive photoconductive target.

1. Introduction

We have been studying a flat image sensor consisting of a field emitter array (FEA) and a high-gain avalanche rushing amorphous photoconductor (HARP) target, with the aim of developing ultrahigh-sensitivity compact HDTV cameras [1], [2], [3]. Our previous experiments on a 90×90 μm pixel Spindt-type FEA image sensor with an 8-μm-thick HARP target (avalanche multiplication factor of about 80) confirmed that the sensor could stably reproduce images and the sensitivity of the HARP target could be utilized [3]. However, for practical purposes, a high-resolution and ultrahigh-sensitivity sensor with smaller pixels and a thicker HARP target must be developed. As a step toward our goal, a 50×50 μm pixel magnetic focus FEA image sensor with a 15-μm-thick HARP target was fabricated and tested.

This paper describes the design concept of the prototype sensor. The prototype's image pick-up characteristics are also discussed.

2. Operating principle

Figure 1 shows the operating principle of the magnetic focus FEA image sensor with the HARP target. The sensor consists of a Spindt-type FEA [4], [5], a mesh electrode, and a HARP target, in close proximity to each other, and permanent magnets are set

outside the sensor. The HARP target converts incident light into electron-hole pairs. The number of holes is increased by the internal avalanche multiplication effect [6], and a charge (hole) pattern corresponding to the optical image is formed at the electrons' scanning side of the HARP target. Electrons emitted sequentially from each pixel of the FEA are, on the other hand, drawn to the HARP target side by the high potential of the mesh electrode, and are focused on the HARP target by a magnetic field between the FEA and the HARP target. The output signal current is obtained by recombining holes accumulated on the HARP target and scanning electrons emitted from the FEA.

3. Design

Electrons emitted from a Spindt-type field emitter (FE) tip have a large divergence of up to 20-30° [7]. As a pixel area decreases, it becomes increasingly difficult to obtain an adequate resolution for the pixel size because of the large divergence of scanning electrons. To overcome this problem, the spread of scanning electrons in the FEA image sensor with magnetic focusing capability was investigated. Specifications of the prototype sensor were also determined by the simulation's results.

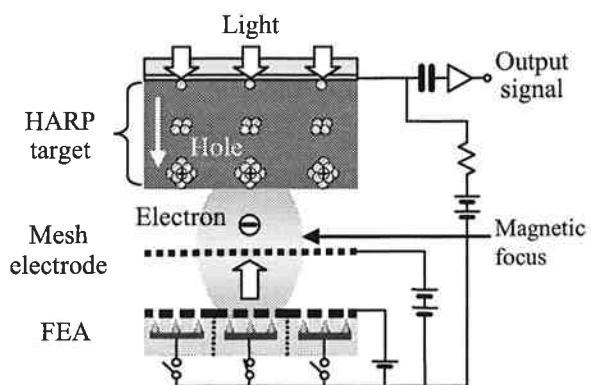


Fig. 1. Operating principle of FEA image sensor

3.1 Design concept

The electron spread in a magnetic field was calculated by using a simplified model shown in Fig. 2. We assumed that

- 1) The gate electrode of the Spindt-type FEA, the mesh electrode and the HARP target are flat planes arranged parallel to the x - y plane.
- 2) $V_m > V_g > 0$ and $V_m > V_t \geq 0$, where V_m is the mesh voltage, V_g is the gate voltage and V_t is the surface potential at the electrons' scanning side of the HARP target.
- 3) Electrons, which have an initial velocity v_{gate} proportional to the square root of the gate voltage V_g and the divergence angle θ ($90^\circ > \theta \geq 0$), are emitted from a point (a virtual emitter tip) on the plane of the gate electrode.
- 4) $v_{xgate} = v_{gate} \cdot \sin \theta \geq 0$, $v_{ygate} = 0$ and $v_{zgate} = v_{gate} \cdot \cos \theta > 0$, where v_{xgate} , v_{ygate} and v_{zgate} are initial velocities of the electron in the x -, y -, and z -directions, respectively.
- 5) A uniform magnetic field with a flux density of B is applied parallel to the z -axis.

The electron spread on the HARP target Df under the above condition is given by Eqs. (1)-(4), because the electron trajectory projected on the x - y plane circulates when the electron is emitted from the virtual emitter tip with the divergence angle θ_{max} , as shown in Fig. 2.

$$Df = 2r \cdot \left| \sin \left(\frac{\omega}{2} Tgt \right) \right| \quad (1)$$

$$r = \frac{m \cdot v_{xgate}}{eB} = \frac{1}{B} \sqrt{\frac{2mV_g}{e}} \sin \theta \quad (2)$$

$$\omega = \frac{v_{xgate}}{r} = \frac{eB}{m} \quad (3)$$

$$Tgt = \sqrt{\frac{2m}{e}} Lgm \left(\frac{\sqrt{V_m - V_g \sin^2 \theta} - \sqrt{V_g} \cos \theta}{V_m - V_g} \right) + \sqrt{\frac{2m}{e}} Lmt \left(\frac{\sqrt{V_m - V_g \sin^2 \theta} - \sqrt{V_t - V_g \sin^2 \theta}}{V_m - V_t} \right) \quad (4)$$

, where r is the radius of the circular motion, ω is the cyclotron angular frequency (radian per second), Tgt is the flight time of the electron, e is the charge of an electron and m is the mass of an electron.

The following condition must be satisfied for the existence of a solution to Eq. (1) and/or (4).

$$V_t - V_g \cdot \sin^2 \theta \geq 0 \quad (5)$$

This means that all electrons emitted from the virtual emitter tip reach the HARP target when

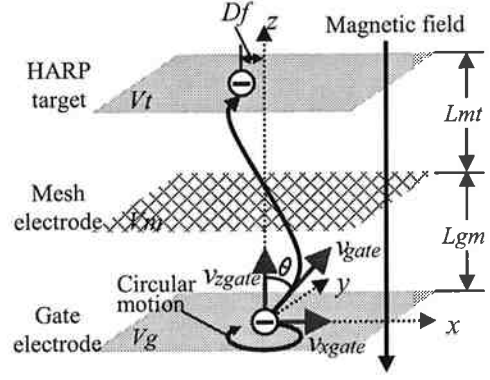


Fig. 2. Simulation model of magnetic focus sensor

$V_t \geq V_g$, and electrons with a divergence angle lower than θ_{max} , which is given by Eq. (6), reach the HARP target when $V_t < V_g$.

$$\theta_{max} = \sin^{-1} \sqrt{\frac{V_t}{V_g}} \quad (6)$$

Figure 3 shows the maximum electron spread on the HARP target plotted against the flux density of the magnetic field, as a parameter of the surface potential of the HARP target. In this simulation, the distance between the gate electrode and the HARP target was 1.8 mm, and the mesh electrode applying a voltage of 300 V was set midway between the gate electrode and the HARP target. A voltage of 50 V was applied to the gate electrode. After θ_{max} for each surface potential of the HARP target was calculated by Eq. (6), the maximum spread of electrons emitted from the virtual emitter tip with divergence angles of 0 to θ_{max} was sought for each flux density by using Eqs. (1) - (4). Local minimum values of the electron spread, which show focusing points, appear cyclically with increasing the flux density, and a higher surface potential of the HARP target causes a wider electron spread because the electrons with a larger divergence angle can reach the HARP target. Figure 4 is an example of calculated electron spreads with and without a focusing magnetic field. The flux density of the magnetic field was set to 0.12 T, and the surface potential of the HARP target

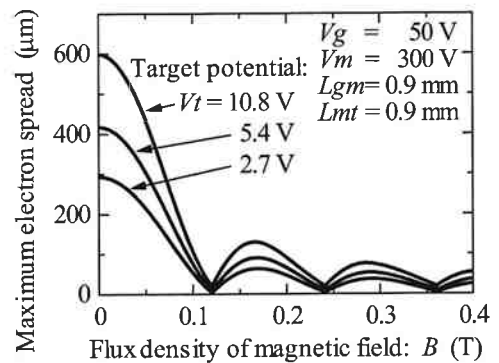


Fig. 3. Dependence of calculated maximum electron spreads on flux density of magnetic field

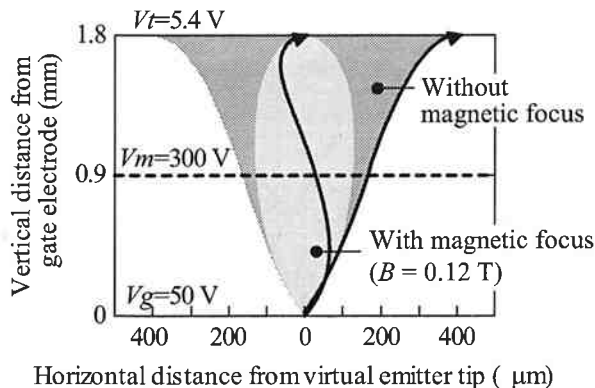


Fig. 4. Calculated electron spreads with and without magnetic focus

was set to 5.4 V, which was equivalent to the potential generated by accumulated charges on the 1-inch (16-mm-diagonal) 15- μm -thick HARP target when the output signal current was about 0.3 μApp . The figure shows that the electron spread on the HARP target can be strongly suppressed by applying an adequate magnetic field to the FEA image sensor.

3.2 Specifications

The number of pixels in the FEA of the prototype is 256 \times 192, and the pixel size is 50 \times 50 μm . 289 Spindt-type FE tips with a gate-hole diameter of about 0.8 μm are placed in a 20 \times 20 μm area of each pixel. The distance between the FEA and the HARP target is 1.8 mm, and the mesh electrode, which has an aperture ratio of about 45%, is midway between the FEA and the target. The thickness of the HARP target is 15 μm . The magnetic focusing system consists of a cylindrical magnet surrounding the prototype sensor and a disc-type magnet at the back of the sensor. The outer diameter, the inner diameter and the height of the cylindrical magnet are 90 mm, 72 mm and 25 mm, and the diameter and the height of the disc-type magnet are 50 mm and 5.3 mm, respectively. This focusing system achieved a flux density of about 0.11 T, the deviation of the flux density in the imaging area of under 0.8% and the ratio of the vertical magnetic field component to the horizontal magnetic field component of under 0.4%.

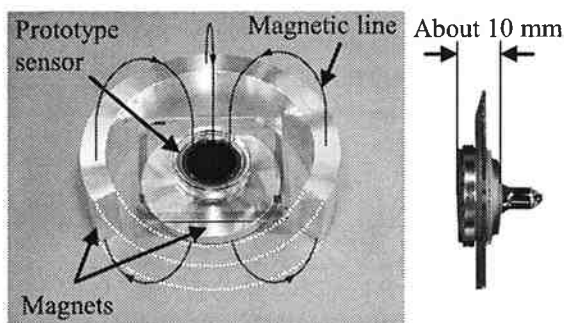


Fig. 5. External view of prototype sensor and its magnetic focusing system



Fig. 6. Reproduced image taken by prototype

Figure 5 shows photographs of the fabricated prototype sensor, which is about 10-mm-thick, and magnetic focusing system.

4. Experiment and discussion

Figure 6 shows a reproduced image picked up by the prototype under an illumination of about 0.1 lx and with the lens iris set at F1.2.

4.1 Operating conditions

Pulses of 0 V and 50 V were applied to gate and cathode lines for vertical and horizontal scanning. The interval and width of these drive pulses basically complied with the NTSC standard. To facilitate the observation, we set the width of horizontal drive pulses to approximately 0.16 μs , which is greater than that of the NTSC standard, and selected one horizontal line twice to obtain expanded images. A voltage of about 300 V was applied to the mesh electrode and a voltage of up to 1580 V was applied to the HARP target.

4.2 Image pick-up characteristics

Figure 7 shows the dependence of output signal current on HARP target voltage under a constant illumination. The signal current saturated at the target voltage of 500 V and abruptly increased above the target voltage of 1200 V, indicating the presence of the avalanche multiplication effect inside the 15- μm -thick HARP target. An avalanche multiplication factor of

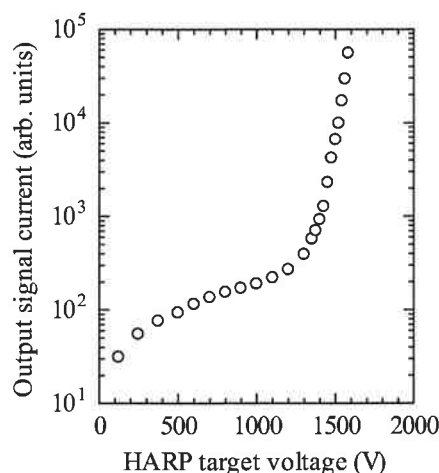


Fig. 7. Dependence of output signal current on HARP target voltage

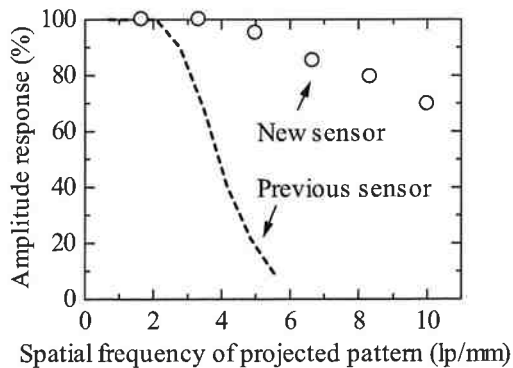


Fig. 8. Resolution characteristics

about 200 was obtained at the target voltage of 1580 V.

Figure 8 shows resolution characteristics of the prototype with focusing magnets and the previous sensor [3]. The resolution was defined by the amplitude response when a black-and-white vertical-stripe pattern with various spatial frequencies was projected on the HARP target. The amplitude response of the prototype was very high compared with that of the previous sensor, and was about 70% at the Nyquist spatial frequency (a spatial frequency of 10 lp/mm or a stripe pitch of 50 μm), and the uniformity of resolution was good. These results approximately agree with the simulation's results and indicate that the sufficient resolution can be obtained by focusing electrons emitted from the FEA onto the target.

Figure 9 shows the dependence of the effective emission current on the gate voltage. The dynamic range of the FEA image sensor is determined by the effective emission current, which contributes to the readout of the accumulated charge on the HARP target. The effective emission current required for the image pick-up operation is estimated to be about 2 μA under ordinary lighting conditions. The result shows that a sufficient dynamic range can be obtained with the prototype's high-density emitter tips, even at a low gate voltage of about 50 V.

Moreover, the capacitive lag of the prototype with 15- μm -thick HARP target was improved compared

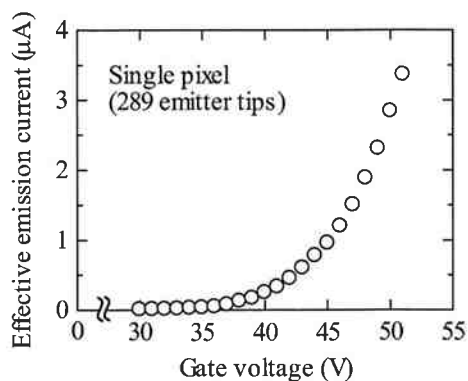


Fig. 9. Dependence of effective emission current on gate voltage

with that of the previous sensor with 8- μm -thick HARP target. This is because that the capacitive lag is determined by the product of the capacitance of the HARP target and the equivalent resistance of scanning electrons, and the capacitance of the HARP target decreases with increasing the target's thickness.

5. Conclusions

The goal of our work has been to develop FEA image sensors for ultrahigh-sensitivity compact HDTV cameras that can be used in various fields such as broadcasting, medicine, security, and natural science.

Our experimental results on the 50 \times 50 μm magnetic focus prototype sensor with the 15- μm -thick HARP target revealed that the prototype sensor could obtain both high sensitivity and enough resolution for its pixel size by focusing electrons emitted from the FEA onto the HARP target.

We plan to develop new FEAs with a large number of much smaller pixels and practical focusing systems toward the goal.

References

- [1] M. Nanba, T. Yamagishi, S. Okazaki, K. Tanioka, K. Takayama, M. Tanaka, and S. Itoh: "Beam characteristics of a high-gain avalanche rushing amorphous photoconductor field-emitter image sensor", *Appl. Surface Sci.*, 146, pp.251-256 (1999).
- [2] Y. Takiguchi, K. Osada, M. Nanba, K. Miyakawa, S. Okazaki, T. Yamagishi, K. Tanioka, M. Abe, N. Egami, M. Tanaka, and S. Itoh: "128 \times 96 Pixel Image Sensor with HARP Target," *IEICE Trans. Electron.*, E85-C, 11, (2002).
- [3] Y. Takiguchi, M. Nanba, K. Osada, T. Watabe, S. Okazaki, N. Egami, K. Tanioka, M. Tanaka, and S. Itoh: "256 \times 192 pixel field emitter array image sensor with high-gain avalanche rushing amorphous photoconductor target," *J. Vac. Sci. Technol. B* 22 (3), pp.1390-1395 (2004).
- [4] C.A. Spindt, I. Brodie, L. Humphrey, and E. R. Westerberg: "Physical Properties of Thin-film Field Emission Cathodes with Molybdenum Cones," *J. Appl. Phys.*, 47, 12, pp. 5248-5263 (1976).
- [5] S. Itoh, N. Mutoh, M. Tanaka, and T. Tonegawa: "Development of Field Emission Display," *Tech. Digest. 16th IVMC*, I3-1, pp.19-20 (2003).
- [6] K. Tanioka, J. Yamazaki, K. Shidara, K. Taketoshi, T. Kawamura, S. Ishioka, and Y. Takasaki: "An-avalanche-Mode Amorphous Selenium Photoconductor Layer for Use as a Camera Tube Target," *IEEE Electron Device Letters*, EDL-8, 9, pp.392-394 (1987).
- [7] S. Ito, T. Watanabe, K. Ohtsu, M. Taniguchi, S. Uzawa and N. Nishimura: "Experimental Study of Field Emission Properties of the Spindt-type Field Emitter", *J. Vac. Sci. Technol. B*13 (2), pp. 487-490 (1995).